RGR

doi:10.1016/j.jmb.2008.12.035

J. Mol. Biol. (2009) xx, xxx-xxx



Available online at www.sciencedirect.com





Stochastic Gating and Drug-Ribosome Interactions

Andrea C. Vaiana and Kevin Y. Sanbonmatsu*

Theoretical Division, Los Alamos National Laboratory, Mail Stop K710, T-10, Los Alamos, NM 87545, USA

Received 1 August 2008; received in revised form 11 December 2008; accepted 13 December 2008 Gentamicin is a potent antibiotic that is used in combination therapy for inhalation anthrax disease. The drug is also often used in therapy for methicillin-resistant Staphylococcus aureus. Gentamicin works by flipping a conformational switch on the ribosome, disrupting the reading head (i.e., 16S ribosomal decoding bases 1492-1493) used for decoding messenger RNA. We use explicit solvent all-atom molecular simulation to study the thermodynamics of the ribosomal decoding site and its interaction with gentamicin. The replica exchange molecular dynamics simulations used an aggregate sampling of 15 µs when summed over all replicas, allowing us to explicitly calculate the free-energy landscape, including a rigorous treatment of enthalpic and entropic effects. Here, we show that the decoding bases flip on a timescale faster than that of gentamicin binding, supporting a stochastic gating mechanism for antibiotic binding, rather than an inducedfit model where the bases only flip in the presence of a ligand. The study also allows us to explore the nonspecific binding landscape near the binding site and reveals that, rather than a two-state bound/unbound scenario, drug dissociation entails shuttling between many metastable local minima in the free-energy landscape. Special care is dedicated to validation of the obtained results, both by direct comparison to experiment and by estimation of simulation convergence.

Published by Elsevier Ltd.

Keywords: RNA; ribosome molecular dynamics simulation; antibiotics; induced-fit

Edited by D. E. Draper

Introduction

More than 50% of antibiotic compounds used today target bacterial ribosomes, thereby interfering with protein synthesis.1 Anthrax and plague diseases are often treated with a combination of antibiotics that includes gentamicin, an aminoglycoside antibiotic that induces aberrant protein synthesis in bacteria by altering the decoding process. Gentamicin is also used to treat gentamicin-susceptible methicillin-resistant Staphylococcus aureus, the deadly superbug that infects or colonizes nearly 5% of all US hospital patients. Drug-resistant mutations in bacteria and the severe side effects induced by prolonged aminoglycoside treatments in humans call for the development of novel antibiotic compounds that can effectively target the ribosomal decoding center (i.e., the aminoacyl site of the small ribosomal subunit). Understanding the detailed

*Corresponding author. E-mail address: kys@lanl.gov. Abbreviations used: MD, molecular dynamics; PMF, potential of mean force; REMD, replica exchange molecular dynamics.

0022-2836/\$ - see front matter. Published by Elsevier Ltd.

mechanism of the binding and dissociation of gentamicin from the ribosome will aid in the rational design of new aminoglycosides.

Aminoglycoside antibiotics act to lock the reading head of the ribosome (i.e., 16S rRNA nucleotides A1492 and A1493) in place, resulting in widespread misreading errors, malfunctioning proteins, and subsequent death of the bacteria. These two critical universally conserved nucleotides appear to constitute a molecular switch. When a tRNA is not bound to the aminoacyl site (A-site) of the ribosome, the decoding bases (A1492 and A1493) are found to reside inside their helix (small subunit helix 44)³ or found in a disordered state.^{4,5} When a tRNA is bound to the A-site, however, the decoding bases are flipped out of their helix, able to form hydrogen bonds with both the codon and the anticodon. This network of interactions is used by the ribosome to discriminate between cognate and near-cognate tRNAs.6-13 Aminoglycosides bind inside helix 44, locking the decoding bases into their flipped-out state^{2,9,14–19} (Fig. 1a). This configuration mimics the presence of a cognate tRNA, causing the ribosome to accept near-cognate tRNAs and to incorporate incorrect amino acids into the nascent protein.

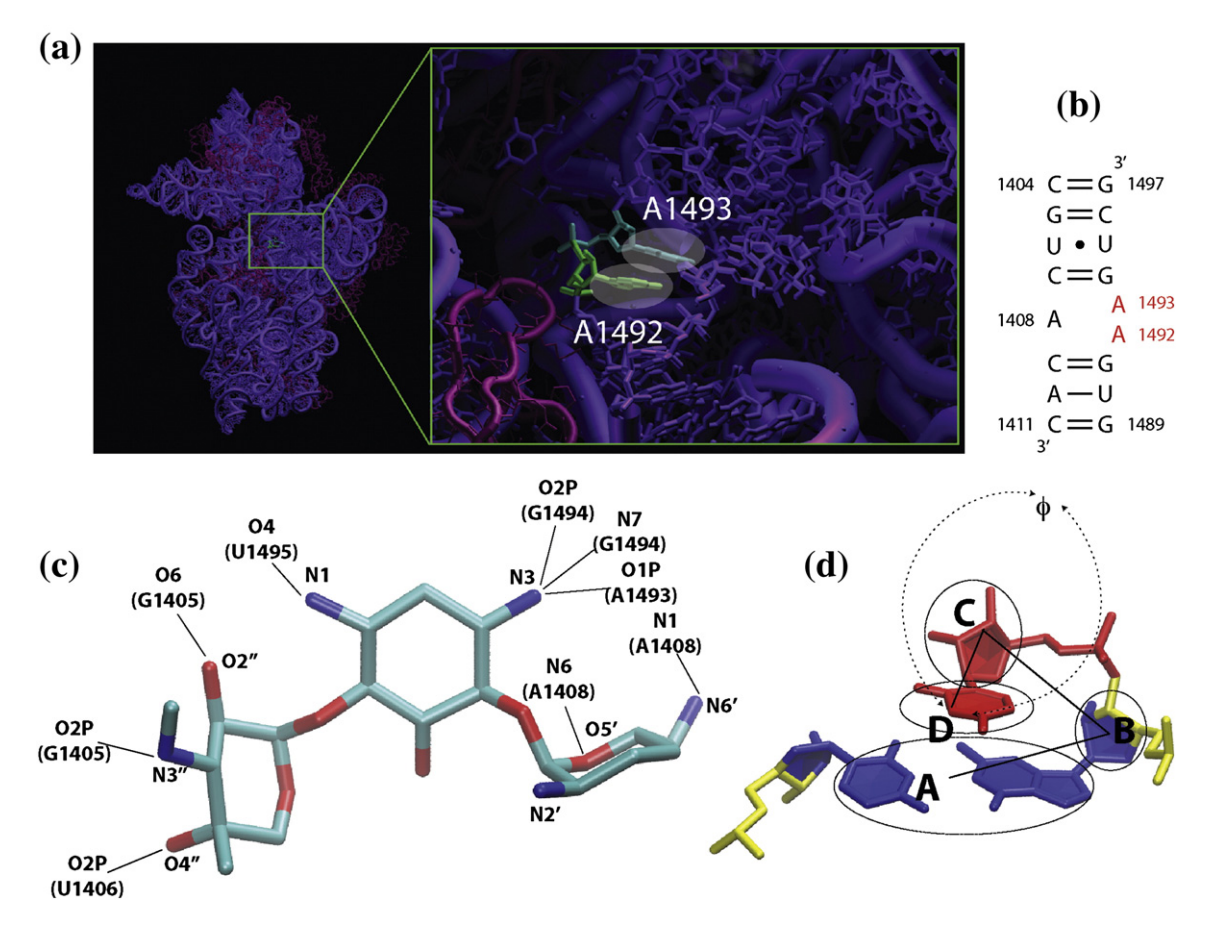


Fig. 1. The ribosomal A-site and gentamicin. (a) The A-site in the context of the 30S ribosomal subunit. (b) Secondary structure of the simulated A-site. (c) Gentamicin structure from Francois $\it et al.$ ¹⁹ The nine crystal contacts to the A-site are evidenced. (d) Definition of the flipping angle φ used here to characterize the flipped-in/flipped-out states of A1492 and A1493, taken from Dang. ²⁰ For a given base, φ is defined as the pseudo-dihedral angle determined by points A, B, C, and D, where A is the center-of-mass of the neighboring base pair, B is that of the neighboring sugar, C is that of the sugar of the base itself, and D is that of the base.

While the mechanism of decoding has been extensively studied, ^{21,22} the detailed molecular and dynamical aspects remain unclear. In particular, although the mechanism of tRNA recognition has been described as an induced fit, it is not clear whether the ligands binding to the ribosome (tRNAs or antibiotics) actually induce a change in the conformation of A1492 and A1493. Instead, a stochastic gating mechanism might operate, where the decoding bases may be continuously flipping in and out of helix 44, ²³ as evidenced by the low density and high *B*-factors often observed in X-ray crystallography structures for these two bases in the absence of ligands. In this case, ligand binding would trap the system in the flipped-out state rather than induce a conformational change. ²⁴

The distinction between induced fit and stochastic gating is a subtle but important one that can lead to significant changes in drug-design strategy. Induced fit involves the creation of a new minimum in the free energy by a ligand–target interaction. The new minimum is rarely, if ever, sampled in ligand-free state. Consistent with previous definitions of induced fit, the binding of the ligand causes a change in the shape of the binding site.²⁵ Stochastic gating

entails the continual fluctuation of the binding site between bound and free conformations in the absence of the ligand. Here, the bound state of the binding site is sampled frequently without the ligand.

Because these characterizations of induced fit and stochastic gating use the words "rarely," "continual," and "frequently," a more precise set of definitions can be formulated using timescales. In the case of the decoding center, the binding site has a bound conformation, with decoding bases flipped out, and a free conformation, with decoding bases flipped inside helix 44. For the purposes of this discussion, we define stochastic gating as the limit that the binding site switches between these configurations much faster than ligand binding. Likewise, we define induced fit as the opposite limit, where the timescale of the binding site conformational change is similar to or slower than ligand binding. The goals of this study are to determine whether base flipping occurs faster than or slower than ligand binding and to address the question "Does gentamicin bind via induced fit or stochastic gating?" In addition, we wish to gain insight into the processes of binding and dissociation to address the question "Does the ligand move directly from the bound state to the unbound state, or does the drug gradually migrate to less and less favorable nonspecific binding sites?"

In a recent experimental study,²⁶ the energetics and dynamics of A1492 and A1493 have been characterized using steady-state and time-resolved fluorescence techniques. Here, Kaul *et al.* find evidence of stacking interactions of A1492 both in the presence and in the absence of aminoglycosides bound to the ribosomal A-site.

Molecular dynamics (MD) simulations have previously been used to investigate drug binding. 27,28 Until now, no theoretical investigation of RNA/drug complexes has reached sufficient sampling (1) to arrive at a full quantitative representation of the free-energy landscape, including transition states, for the flipping of A1492 and A1493, and (2) to elucidate binding/unbinding pathways and relative freeenergy differences along these pathways. The replica exchange molecular dynamics (REMD) methodology used in our present aggregate microsecond timescale simulations is a thermodynamically reversible, enhanced sampling method that can achieve significantly more sampling than an equivalent classical MD simulation. ^{29,30} REMD simulations have been used extensively in the study of peptides and proteins,^{29,31-33} and have proven to give reliable estimates of folding/unfolding free energies and pathways. A recent ground-breaking study of RNA folding has also been performed.34 We note that a limitation to our method is that it is difficult to obtain kinetic information because the algorithm produces simulation trajectories with time-dependent temperatures. Thus, it is not possible to directly calculate rates by counting events. The method only allows one to accurately gauge the relative probability of finding the system in a given state at a given temperature and thus to obtain a free energy for that state. In this context, a more meaningful analysis can be obtained from the free-energy landscape of the system. By comparing the free-energy barriers of base flipping and drug dissociation, we can determine the relative ordering of the timescales and, in turn, whether we are in the induced-fit or stochastic gating regime.

Results

We present two REMD simulations of the ribosomal A-site. Simulation S1 consists of >1 μs (21 ns per replica) total sampling of the empty or "free" A-site. Simulation S2 simulates the gentamicin/A-site complex, consisting of >15 μs (320 ns per replica) total sampling of the gentamicin/A-site complex, representing the "bound" state.

Flipping of A1492 and A1493

The questions of how the A-site switch moves between on and off states and how this is influenced by gentamicin were addressed by calculating onedimensional and two-dimensional free-energy landscapes for the flipping of A1492 and A1493 at 300 K from two REMD simulations (S1 and S2) of the Escherichia coli A-site in the absence and in the presence of gentamicin (Fig. 1c), respectively. A suite of relevant X-ray structures was used as the basis of initial starting conditions distributed throughout the temperature distribution of replicas.^{3,4,8,9,19} Although NMR structures of both the bound state and the unbound state have been solved, X-ray structures were used to determine whether the system would spontaneously relax towards the NMR bound state. 14 The coordinate ϕ (Fig. 1d) describing the flip state for the two adenine nucleotides is defined so that values in the vicinity of $\phi = 0$ correspond to the residue lying inside helix 44 (flipped-in), whereas values of $\phi \sim \pm 180$ correspond to completely flipped-out states. All free-energy values reported are relative to the global minimum of the landscape itself and are expressed in kilocalories per

At a first glance, both landscapes (Fig. 2) appear rugged and, with several local minima, connected by higher free-energy pathways. The morphologies of the two landscapes appear to be very different, although the free-energy values at the minima and heights of the barriers connecting them are comparable.

Convergence of simulations S1 and S2 was estimated by calculating the time dependence of the average deviations $\sigma(t)$ of the two-dimensional potential of mean force (PMF) landscapes:

$$\sigma(t) = \sqrt{\frac{\sum_{i,j} \left(\Delta G(i,j)_t - \Delta G(i,j)_{t_0}\right)^2}{N}}$$
 (1a)

Here, $\Delta G(i,j)_t$ denotes the free energy surface over the $(\phi_{1492}, \phi_{1493})$ plane obtained after time t of the simulation, and $\Delta G(i,j)_{t_0}$ denotes the free-energy surface obtained at time t_0 , where t_0 =0.05 μ s (total sampling) for simulation S1 and t_0 = 2.5 μ s (total sampling) for S2. N is the total number of grid points on the landscape. Similarly, the average statistical fluctuation as a function of time $\zeta(t)$ of the PMF landscapes was estimated as follows:

$$\zeta(t) = \sqrt{\frac{\sum_{i,j} \left(\Delta G(i,j)_t - \Delta G(i,j)_{t-\Delta t}\right)^2}{N}}$$
 (1b)

Results are shown in Fig. 3a and b. Values of $\sigma(t)$ approach a plateau, indicating convergence after $\sim 0.5~\mu s$ in the case of the free A-site and after $\sim 12~\mu s$ in that of the gentamicin-bound A-site complex. In both simulations S1 and S2, $\zeta(t)$ tends to zero and remains below 0.2 kcal/mol in the plateau region. The landscape for the flipping of A1492 and A1493 arising from simulation S1 converges much more rapidly than that of simulation S2. This is not surprising, since the presence of the antibiotic bound to the A-site drastically changes the average flipping time of the decoding bases.

In the absence of gentamicin (Figs. 2a and 4a and c), A1492 is essentially confined to the flipped-in states ($-50 < \phi < 50$), whereas A1493 explores the

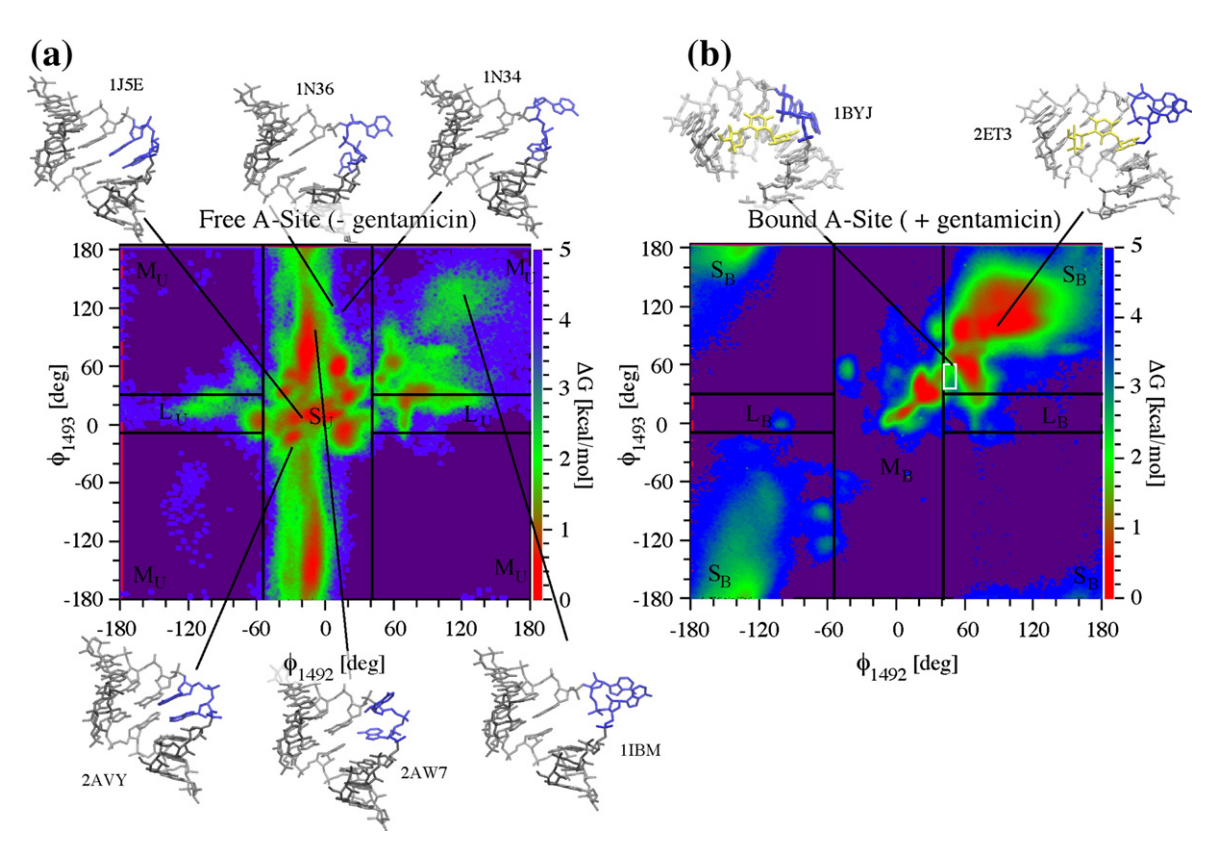


Fig. 2. Two-dimensional free-energy landscapes as a function of base-flipping coordinates $φ_{1492}$ and $φ_{1493}$ resulting from simulations S1 (a) and S2 (b) for the flipping of A1492 and A1493. Starting X-ray structures used for the two simulations and relative Protein Data Bank accession codes are shown along with one NMR ensemble structure (1BYJ). Arrows evidence the position of the corresponding structures on the $(φ_{1492}, φ_{1493})$ plane. The 37 structures from the NMR ensemble for the bound state all lay within the white box in (b). Lines delimiting areas S, M, and L (with subscript U for the unbound state) were obtained by matching time-resolved fluorescence amplitudes from Kaul et al. to the probability amplitudes from simulation S1 of finding the system in areas S, M, and L described in the text (a). The same experimentally calibrated values of $φ_{1492,min}$, $φ_{1493,min}$, $φ_{1492,max}$, and $φ_{1492,max}$ are applied to the free-energy landscape of the gentamicin simulation (subscript B for bound state) in (b).

whole spectrum of ϕ -space. The flipped-out states of A1492 are essentially limited to positive ϕ angles. States with both residues flipped out occur less frequently and are limited to the upper right-hand quadrant of the landscape ($\phi_{1492} > 100$; $\phi_{1493} > 100$). With the exception of this high free-energy region of the plane, flipping motions of A1492 are independent of the state of A1493. Flipping out of A1492 involves the crossing of high free-energy barriers (between 3 and 3.5 kcal/mol), while the barriers for A1493 are significantly smaller (~1.3 kcal/mol). This higher mobility of A1493 is in agreement with available structural and biochemical data on the ribosomal A-site. 9,26 Movie 1 (see Supporting Information) shows a typical example of flipping events for both A1492 and A1493 in the context of the 30S ribosomal subunit during S1 simulation (gentamicin-free). We cannot overemphasize that this movie displays a minute fraction of our total simulation data (less than 1/1000). Because of the large amount of data, no single trajectory is representative of the entire data set. We observe thousands of events such as those displayed in the movie (>10,000 base-flipping events). The entire

data set is described by the free-energy landscapes discussed above. The movie shows an example of what a flipping event might look like. The movie represents a single replica moving from $T \sim 300$ K to higher temperatures and then back to room temperature. What can be seen is a typical illustration of the REMD methodology at work: at lower temperatures, the global free-energy minimum (most probable states) corresponds to both A1492 and A1493 flipped in; at higher temperatures, the barriers for flipping are more easily overcome and both bases can flip freely; as the system returns to lower temperatures, it has a higher probability to be in a flipped-in state, as seen at the end of the movie.

In order to obtain the relevant timescale for the flipping out of A1492 from the minimum of Fig. 4a, angular diffusion and drift coefficients $[D(\phi_{1492}), v(\phi_{1492})]$ were derived from simulation S1 from the short timescale evolution of the first two moments of the flipping angle ϕ_{1492} , as described in Kopelevich *et al.*, ³⁶ Yang *et al.*, ³⁷ and McCammon *et al.* ³⁸ The validity of the obtained diffusion and drift coefficients was verified by rederiving the one-dimensional PMF of Fig. 2a within the global minimum

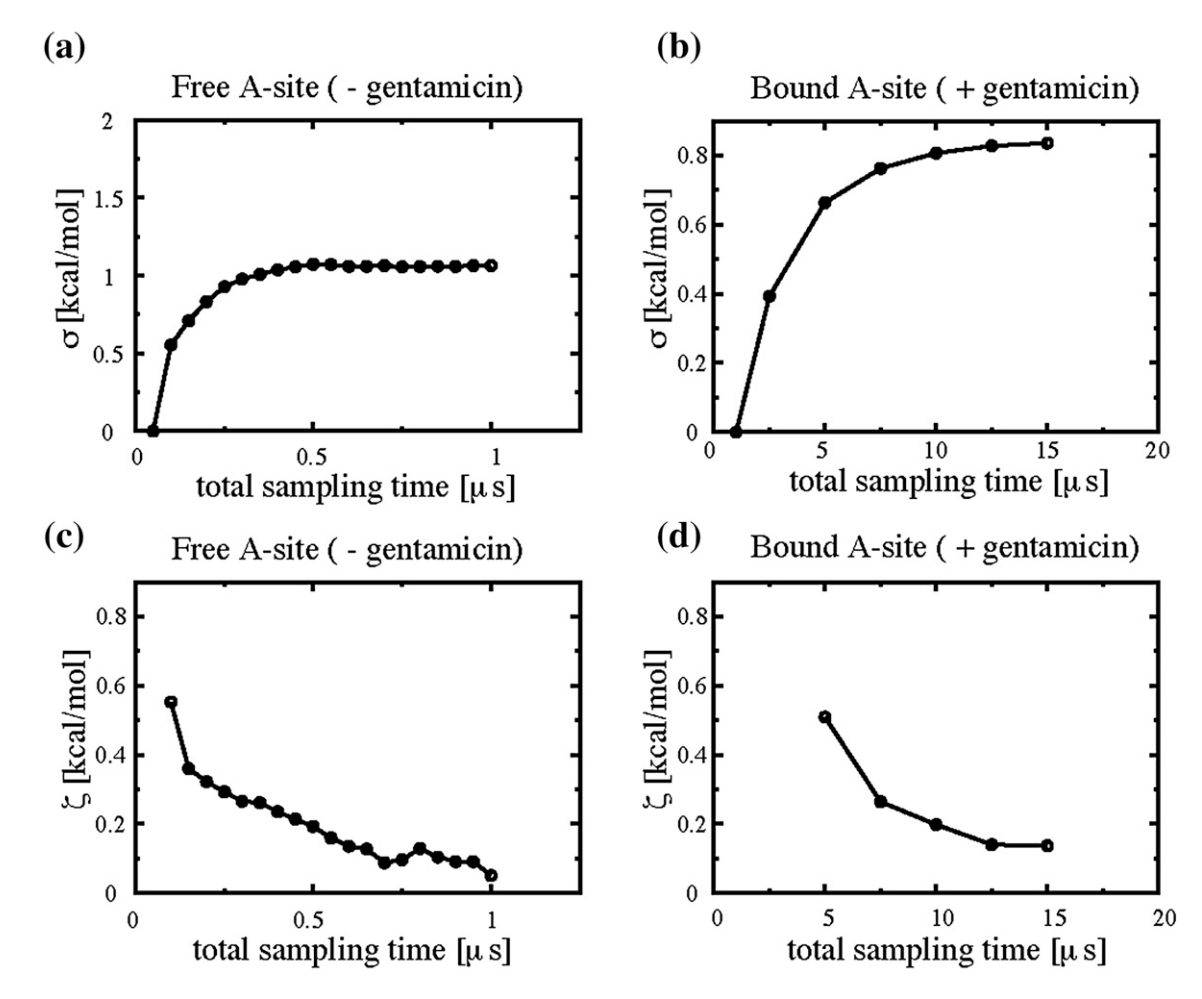


Fig. 3. Convergence and fluctuation estimates for the free-energy landscapes of Fig. 2. (a and c) Simulation S1. (b and d) Simulation S2. Convergence was estimated by calculating the deviation $\sigma(t)$ (Eq. (1a)) of the two-dimensional cumulative PMF landscapes $\Delta G_{\rm flip}(\phi_{1492},\phi_{1493})_t$ obtained after time t from those obtained at time t_0 . Values of σ approach a plateau, indicating convergence after \sim 0.5 μs in the case of the free A-site and after \sim 12 μs in the case of the gentamicin/A-site complex. Fluctuations $\zeta(t)$ were similarly derived using Eq. (1b). Values of $\zeta(t)$ remain below 0.2 kcal/mol in the plateau region for both simulations.

(between points A and B in Fig. 2a). This was done using an equilibrium probability distribution derived by substituting $D(\phi_{1492})$ and $v(\phi_{1492})$ into the solution of the steady-state Fokker–Planck equation and not directly from the simulation data. The blue solid curve in Fig. 4a is the effective free energy 36 $G_{\rm FP}$ resulting from this calculation; the green line represents the homogeneous diffusion approximation 36 $G_{\rm FP}^{0}$ to the effective free energy.

In Fig. 4a, both G_{FP}^0 and G_{FP} match the G_{MD} curve closely for values of ϕ_{1492} inside the minimum, confirming the validity of the calculated diffusion/drift constants. An estimate based on the average diffusion constant $\langle D(\phi_{1492}) \rangle = 7.5 \text{ deg}^2/\text{ps}$, and a free-energy barrier in the range of 2.3–2.4 kcal/mol yields escape times from the minimum of Fig. 4a between 560 ps and 660 ps.

The presence of gentamicin causes a dramatic shift in the equilibrium from the flipped-in state to the flipped-out state for both A1492 and A1493. The highest number of configurations is found in the main flipped-out minimum (upper right-hand corner of the landscape in Fig. 2b). As mentioned above, these configurations are among those accessible to the free A-site. Interestingly, some partially flipped-in states (for both A1492 and A1493) still occur with relatively high frequency, as evidenced by local free-energy minimum that displays φ values between 30° and 50°. Upon visual inspection of the trajectories, these states are observed to occur at times in which the gentamicin exits the binding site completely. Unlike the free A-site, the pathway connecting flipped-in states with flipped-out states follows the diagonal of the plane, indicating a high degree of correlation in the flipping-in/ flipping-out of the two residues. An example of this concerted flipping can be seen in Movie 2 (Supporting Information).

Gentamicin binding and unbinding pathways

The $>15~\mu s$ of aggregate-enhanced sampling achieved in simulation S2 makes this the first allatom simulation of a drug/RNA complex to allow a

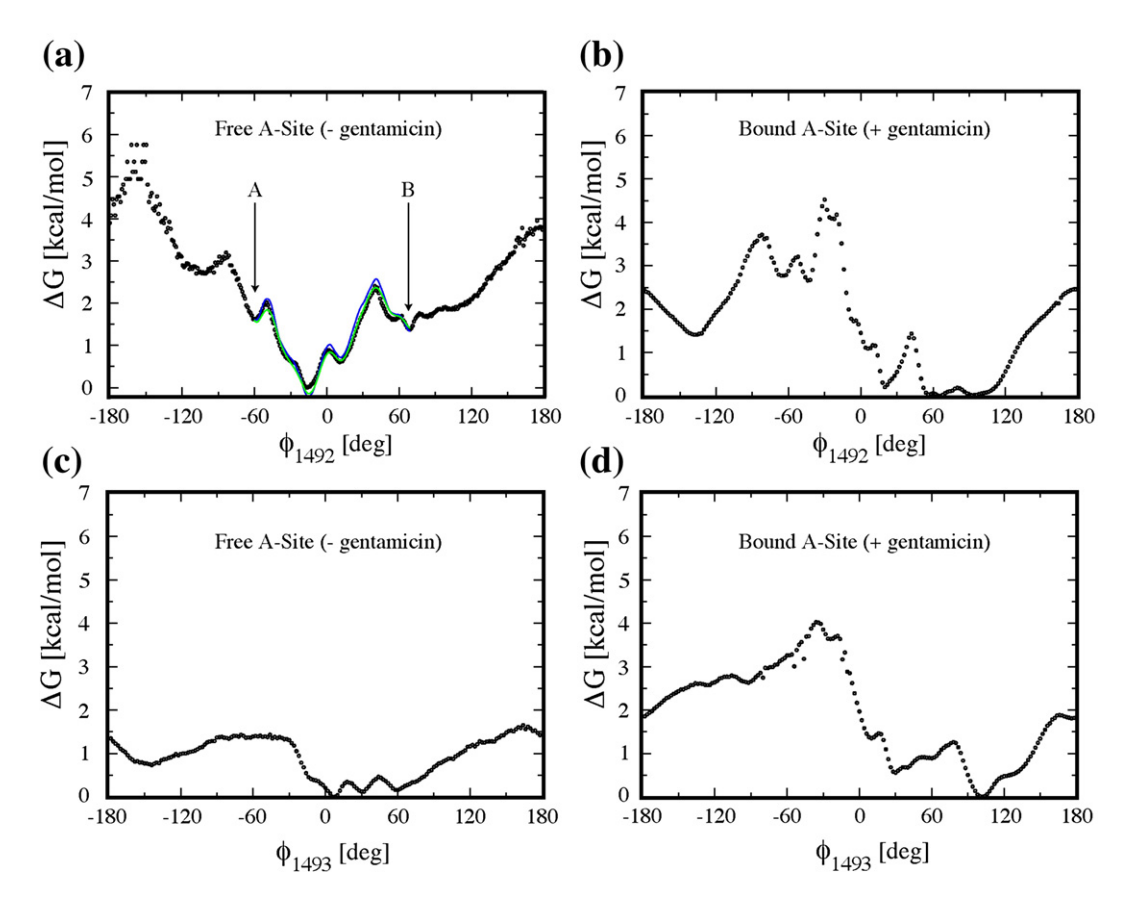


Fig. 4. One-dimensional free-energy landscapes as a function of base-flipping coordinates ϕ_{1492} and ϕ_{1493} resulting from simulations S1 (a and c) and S2 (b and d) for the flipping of A1492 and A1493. A1492 is confined to mostly flipped-in states in the absence of gentamicin (a), whereas A1493 is highly mobile (c). Gentamicin binding to the A-site shifts the equilibrium from the flipped-in states to the flipped-out states of both A1492 and A1493. The blue curve in (a) represents the effective free energy as rederived between points A and B from simulation S1 using the solution of the steady-state Fokker–Planck equation and not directly from the simulation data. The green curve in (a) represents the homogeneous diffusion approximation 36 to the effective free energy. Both curves are in good agreement with the free energies derived directly from Eq. (3) (black circles).

detailed statistical analysis of the specific binding process. Indeed, many of the trajectories exhibit multiple complete unbinding and partial rebinding events in which the center-of-mass of the gentamicin molecule drifts as far as 10 Å from the binding site and successively reenters the binding site, exploring a wide range of available configurations. Movie 2 (Supporting Information) shows an example of such an unbinding/rebinding sequence. We observe approximately 1000 events.

In order to obtain a quantitative picture of the binding mechanism, the two-dimensional PMF, $G(R_{\rm CM}, R_{\rm X}, T)$ at T=300 K, was calculated from simulation S2 as a function of the two reaction coordinates $R_{\rm CM}$ and $R_{\rm X}$ defined in Methods (Fig. 5a). $R_{\rm CM}$ gives the center-of-mass distance of gentamicin from the binding site, while $R_{\rm X}$ characterizes the native contacts found in the X-ray structure. At low values of $R_{\rm CM}$, $R_{\rm X}$ is a measure of how closely the orientation of gentamicin in the binding pocket matches that of the crystallographic structure. This is particularly useful in evaluating the relative probability of finding bound conformations ($R_{\rm CM}$ ~0) where the drug is still in the binding pocket, but not

in the same orientation as in the experimental structure.

For large values of R_{CM} , R_X approaches R_{CM} . The binding free-energy landscape (Fig. 5a) has a funneled shape, with the global minimum (labeled A in Fig. 5) corresponding to the crystallographic structure ($R_X \sim R_{CM} \sim 0$ Å). In the vicinity of the binding site region (R_{CM} < 3.0 Å), the landscape is very rugged and characterized by the presence of several local minima. Two of these minima in particular, points B and C in Fig. 5a, represent kinetic traps within the binding site itself where the centerof-mass of the gentamicin molecule is very close to the "native" state ($R_{\rm CM} \sim 0$ Å), but the orientation of the ligand does not match the crystallographic structure ($R_X \sim 1.6$ Å and $R_X \sim 2.25$ Å). The lowest free-energy pathway for the initial stages of gentamicin unbinding initially moves along the $R_{CM}=0$ Å axis and crosses an ~ 4.5 -kcal/mol barrier in the vicinity of $R_X = 0.8$ Å. Thus, the free-energy barrier for gentamicin unbinding (>4 kcal/mol) is at least twice that of the barrier for base flipping (1-2 kcal/ mol) in the absence of gentamicin. Assuming that the rates are proportional to $\exp(-\Delta G/kT)$, the

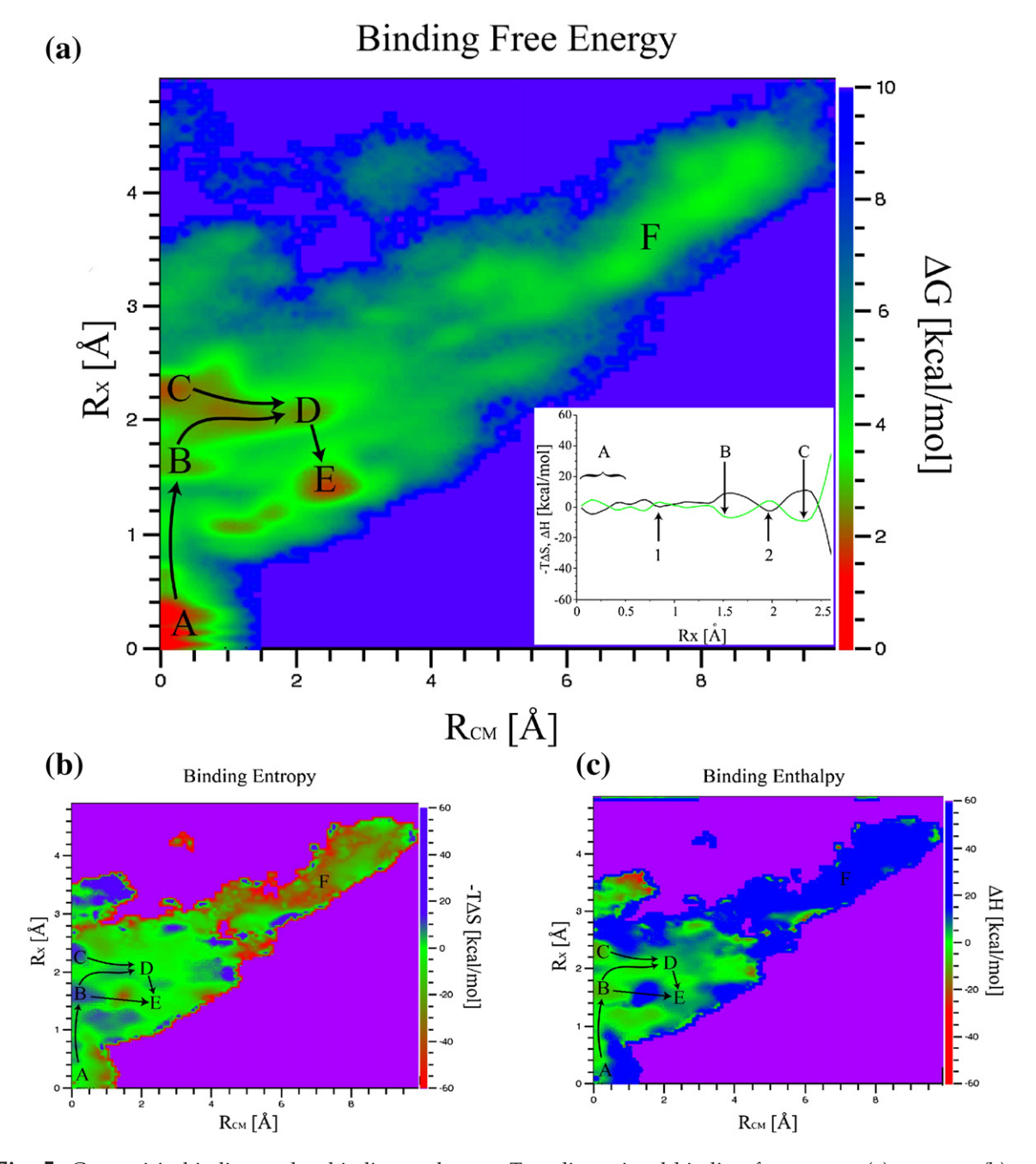


Fig. 5. Gentamicin binding and unbinding pathways. Two-dimensional binding free energy (a), entropy (b), and enthalpy (c) landscapes obtained at T=300 K are shown as a function of coordinates $R_{\rm CM}$ and $R_{\rm X}$. It should be noted that direct entropic contributions to the free energy are plotted here ($-T\Delta S$). The global minimum of the binding free-energy landscape, labeled A, corresponds to the crystallographic structure ($R_{\rm X} \sim R_{\rm CM} \sim 0$ Å). Inside the binding site ($R_{\rm CM} < 3.0$ Å), the landscape is very rugged and characterized by the presence of several local minima. Points B through E are kinetic traps within the binding site. The lowest free-energy pathways connecting the minima are evidenced. Entropy-dominated/enthalpy-dominated regions (red to yellow areas of (b)/(c), respectively) are scattered across the landscape and not limited to bound states. The inset in (a) shows the entropy (black) and enthalpy (green) contributions to the free energy along the path connecting minima A, B, and C. Points 1 and 2 along the path are typical examples of entropy-shuttling states. States within minima labeled B and C are enthalpy-dominated, whereas those labeled D, E, and F are entropy-dominated. Escape to the unbound region F involves crossing several barriers, where entropy "shuttling" plays a crucial role. It should be noted that the range spanned by the energy scales is very different for the free energy and for its entropic/enthalpic components. This is at the origin of the well-known phenomenon of entropy-enthalpy compensation³⁹ that is clearly visible in the inset of (a).

unbinding rate is more than an order of magnitude slower than the flipping rate, consistent with the stochastic gating mechanism. We note that the

crossing of this barrier involves an initial breaking of the hydrogen bonds between the RNA and the ligand, without significant movement of the gentamicin center-of-mass in the binding site. The most probable (lowest free energy) escape pathways leading away from the two kinetic traps (2 and 3 in Fig. 5a) move along a region of roughly constant $R_{\rm X}$ and increasing $R_{\rm CM}$, implying the existence of preferred unbinding orientations. The increase in entropy along this pathway enables gentamicin to tumble within the binding site until it reaches an orientation favorable for its center-of-mass to escape from the binding site. This process is analogous to "jiggling" a key until the correct orientation is found to fit into the keyhole. The highest saddle point of the free-energy landscape along the escape pathway leading to the region labeled F in Fig. 5, positioned at $R_{\rm CM} \sim 4.2$ and $R_{\rm X} \sim 3.0$, is ~ 5.5 kcal/mol above the global minimum.

In state A of Fig. 5, both bases exist in the flippedout configuration with the drug in the binding pocket, as in the X-ray structure. State B has A1492 flipped out and A1493 flipped in, interacting with ring 1 of gentamicin. States C and D are similar. Both states show A1492 and A1493 flipped out with much weaker gentamicin–ribosome interactions compared to states A and B. State E shows both A1492 and A1493 with few interactions between the antibiotic and the ribosome. State F shows both bases flipped in with the antibiotic outside of the binding site. It appears that state B may facilitate dissociation by freeing ring 1 from the binding site (Fig. 6).

Entropic and enthalpic contributions to the freeenergy landscape at T = 300 K were obtained from the temperature dependence of the free energy, as

explained in Methods. Free-energy values were calculated as a function of R_{CM} , R_X , and T for the 10 replicas in the vicinity of T = 300 K (T = 283.8 K to T = 315.2 K). Points sampled at more than 4 of the 10 temperatures were used to obtain values of $\Delta H(R_{\rm CM})$, $R_{\rm X}$, 300 K) and $-T\Delta S(R_{\rm CM}, R_{\rm X}, 300 \text{ K})$ by fitting Eq. (4) as described in Nymeyer *et al.*⁴⁰ Enthalpy and entropy contributions to the free energy are shown as a function of R_{CM} and R_{X} in Fig. 5b and c, respectively. In Fig. 5c, the entropic contribution to the free energy is expressed as $-T\Delta S$; the minus sign assures that this is the direct contribution to the free energy. Thus, with this definition of entropy contribution, if, at any given point of configurational space, $-T\Delta S$ is lower (in its numerical value) than ΔH , the entropy contributes more than the enthalpy to stabilizing (lowering the free energy) the system in that point. The most dominant (stabilizing) effect on the free energy is due to the lower of the two contributions. In this sense, we will refer to entropy-dominated regions as opposed to enthalpy-dominated regions of the landscape.

It should be noted that the range spanned by the energy scales in Fig. 5 is very different for the free energy and for its entropic/enthalpic components. This should not be surprising; it is a well-known fact in equilibrium thermodynamics that, for any given system, fluctuations in free energy are expected to be much smaller than those in enthalpy/entropy. This leads, as can be seen in Fig. 5, to the well-known phenomenon of entropy—enthalpy compensation.³⁹

Enthalpy-dominated regions (yellowish green to red areas of Fig. 5c) are scattered across the

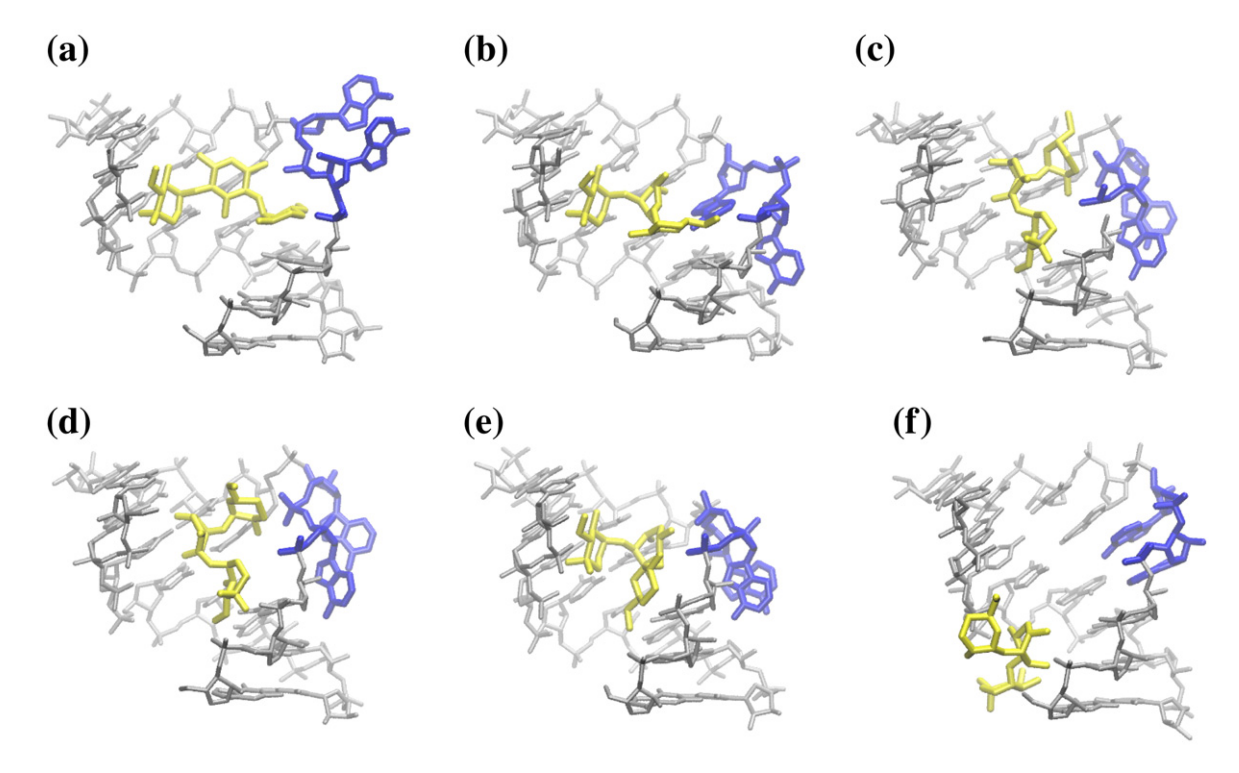


Fig. 6. Representative structures of gentamicin and RNA in states labeled (a) through (f) in Fig. 5 extracted from simulation S2. Gentamicin is shown in yellow; decoding bases A1492 and A1493 are shown in blue.

landscape and not limited to bound states. The same is true for the entropy-dominated regions (yellowish green to red areas in Fig. 5b). The major free-energy local minima basins are not all found in enthalpy-dominated regions. In particular, states within minima labeled D and E are entropy-dominated, with $(-T\Delta S)_D \sim -1$ kcal/mol, $(-T\Delta S)_{\rm E} \sim -2$ kcal/mol, $\Delta H_{\rm D} \sim 2$ kcal/mol, and $\Delta H_{\rm E} \sim 3$ kcal/mol. On the contrary, states within the other two minima in the binding site, B and C, are enthalpy-dominated; however, the barriers between these minima are entropy-dominated (Fig. 5a, inset). The completely unbound states in the region, marked F, of the landscape are highly entropy-dominated $[(-T\Delta S)_F \sim -23 \text{ kcal/}]$ mol; $\Delta H_{\rm F} \sim 28$ kcal/mol)].

Discussion and Conclusions

Gentamicin gradually migrates to less and less favorable nonspecific interaction sites

From the decomposition of the free energy into entropic/enthalpic contributions, it becomes clear that the abovementioned "keyhole" effect is much more general in character: along all the minimum free-energy pathways connecting the most prominent free-energy minima, the system must move through a highly entropy-dominated region (ΔH >0 and $-T\Delta S < 0$), leading to a saddle point before descending into the next minimum. This entropic "shuttling" between free-energy minima does not depend on the specific character (entropy-dominated or enthalpy-dominated) of the minima involved and does not imply crossing of purely entropic barriers. The barriers are often mixed in character with locally entropy-dominated and enthalpy-dominated regions. We emphasize that enthalpy plays a key role in drug dissociation, providing a pathway of local minima near the binding site for the entrance and exit of the drug. In our simulations, entropy appears to facilitate movement between these local minima during the dissociation process.

Gentamicin-ribosome interactions occur via stochastic gating rather than via induced fit

Because the free-energy barrier for base flipping in the free state is much lower than the barrier for drug dissociation, we conclude that the timescale of base flipping is much faster than the timescale of drug dissociation in our simulations. Consistent with this observation, we observe a quite weak correlation between base flipping and drug dissociation for a given replica (the correlation coefficient between $R_{\rm CM}$ and φ is approximately -0.1). Some degree of correlation is to be expected due to a steric effect: there is not enough space in the A-site for the two adenine nucleotides and the antibiotic to be simultaneously located within the binding site. So for the states in which the adenine nucleotides

are flipped in, the gentamicin must move out of the binding site.

Comparison with experiment

The higher mobility of A1493 is in general agreement with available crystallographic data: among the six structures used in this study, four have A1493 in a flipped-out state, whereas all but one has A1492 in a flipped-in state. It is this extended mobility of A1493 that makes the ribosomal A-site a very atypical adenosine bulge structure. The presence of gentamicin in the binding site drastically reduces the mobility of A1493 and shifts the preferred orientation of both adenine nucleotides to the flipped-out configuration. Interestingly, in the presence of gentamicin, conformations close to that of the X-ray structure correspond to the global freeenergy minimum, while those corresponding to the 37 NMR structures lie on the pathway connecting the flipped-in and flipped-out minima, as is expected from solution structures representing thermodynamic averages over all possible configurations (Fig. 2b). 14,19

The possibility of stacked (flipped-in) conformations of A1492, even in the presence of aminoglycoside drugs bound to the A-site, has been experimentally verified by Kaul *et al.* using a fluorescent analog of the ribosomal A-site, in which A1492 was substituted by a 2-aminopurine. In particular, the timeresolved fluorescence experiments described in Kaul *et al.* indicate the existence of three distinct fluorescent states (with different lifetimes and amplitudes) both for the empty A-site analog and for the four aminoglycoside/A-site complexes. The three different fluorescent states correspond to different types of stacking interactions of the 2-aminopurine with the surrounding environment. Here we start from the working hypothesis described schematically in Fig. 7.

The normalized amplitudes for the three distinct fluorescent states in the absence of bound antibiotics ($a_{LU}=0.076$, $a_{MU}=0.098$, and $a_{SU}=0.826$) were used to calibrate the free-energy landscape of Fig. 2a to the three states, as described in Methods. The experimentally calibrated values of $\phi_{1492,min}$, $\phi_{1493,min}$, $\phi_{1492,max}$, and $\phi_{1493,max}$ were then applied to the free-energy landscape of the gentamicin simulation (simulation S2; Fig. 2b), and the corresponding amplitudes were calculated from the probability distribution $P(\phi_{1492}, \phi_{1493},$ 300 K). Amplitudes in the presence of gentamicin were $a_{LB}' = 0.0034$, $a_{MB}' = 0.160$, and $a_{SB}' = 0.837$. These values are in the range of those measured for other antibiotics of the same class, 26 with gentamicin values closer to those of neomycin $(a_L = 0.017, a_M = 0.139, \text{ and } a_S = 0.844)$. Interestingly, of the four aminoglycosides studied in Kaul et al., neomycin is the one that exhibits antimicrobial activity closest to that of gentamicin.²⁶

Results from simulation S1 were also compared to fluorescence anisotropy decay measurements. ²⁶ The anisotropy decay time measured for the free A-site is

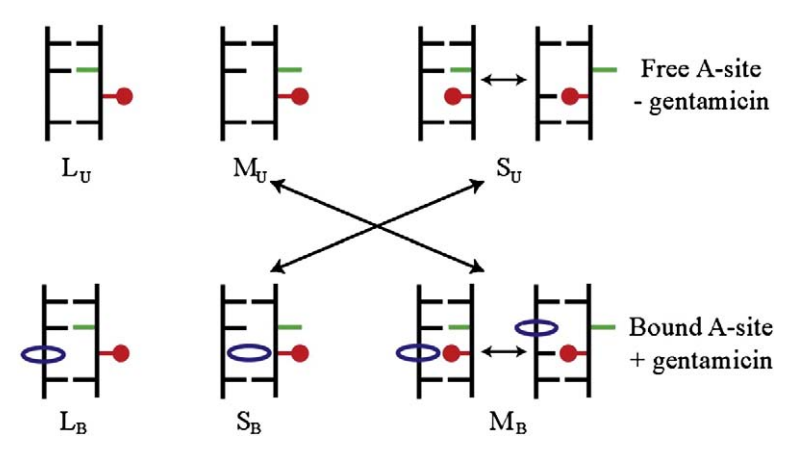


Fig. 7. Schematic representation of hypothetical fluorescent states for the A1492/2AP1492-substituted A-site (top) and aminoglycoside/ A-site complexes (bottom) as measured in Kaul *et al.*³⁵ The 2AP in position 1492 is represented in red, A1493 is represented in green, and the antibiotic is represented in blue. The longest measured lifetime (lowest quenching probability), labeled L_U for the unbound state and L_B for the bound state, corresponds to configurations with 2AP1492 flipped out and with A1493 flipped

in in both the bound state and the unbound state. In the absence of bound antibiotics, the shortest measured lifetime (highest quenching probability), labeled S_U , corresponds to highly populated intrahelical stacked conformations of 2AP1492. Aminoglycoside binding to the A-site shifts the highly populated states to extrahelical stacked S_B states of 2AP. In the absence of aminoglycosides to the A-site, the experimental lifetimes are: (i) $S_U, \tau_S = 0.31$ ns, which corresponds to an intrahelical stacking of A1492 (highly quenched state); (ii) $M_U, \tau_M = 2.85$ ns, which corresponds to extrahelical stacking between A1492 and A1493; and (iii) $L_U, \tau_L = 9.21$ ns, which corresponds to configurations in which A1492 is not involved in stacking interactions (i.e., A1492 in an extrahelical state with A1493 inside the helix). The relative fluorescence amplitudes, normalized by the total intensity, give the relative populations of these three states.

reported to be 540 ± 150 ps. This decay time is linked to the mobility of the 2-aminopurine, specifically to the interconversion between the flipped-in and the flipped-out states of A1492. The escape time from the flipped-in states estimated from our simulations was 610 ± 100 ps, in reasonable agreement with the fluorescence anisotropy decay measurements.

Isothermal titration calorimetry profiles of paromomycin bound to a ribosomal A-site model oligonucleotide, performed by Kaul et al., exhibit a certain amount of nonspecificity in the binding of the drug to the RNA.³⁵ On the other hand, the complex picture emerging from the rugged binding free-energy landscape of the simulated gentamicin/ A-site system also shows significant evidence of unspecific binding. In practice, the simulation data provide a more detailed representation of nonspecifically bound states, evidencing the multistate character of the kinetics within and around the binding site. The simulation, in this sense, complements the isothermal titration calorimetry data in resolving the complex landscape of the unspecific binding, but cannot access the completely unbound states in which the drug and the RNA are at a distance of much more than 10 A apart.

Enthalpic and entropic contributions to free energy

The complexity of the free-energy landscape itself makes it difficult to describe the enthalpy and entropy of binding in terms of bound and unbound states. The free-energy landscape surrounding each local minimum is intermixed with regions where the constant interplay between entropy and enthalpy allows ligand escape. This interplay cannot be simplified into switching between bound and unbound states (or between any other dual classification of states). While the details of the binding

free-energy landscape are a specific characteristic of this particular gentamicin/RNA complex, the complexity and ruggedness of the landscape itself are not. The same general characteristic complexity exists in systems that range from protein–protein interactions, ⁴¹ to small ligand systems, to water molecules interacting with biological molecules. ^{28,42}

Implications for high-performance computing studies

From our sampling convergence estimates (Fig. 3), the gentamicin-bound simulation S2 is near equilibrium after 15 μs of total REMD sampling (320 ns per replica); however, it is likely that similar estimates of changes in free energy for tRNA binding, or even tRNA anticodon stem loop binding, will require much more sampling than that achieved in this study due to the large size of the tRNA ligand. Previous estimates of free energies of tRNA binding have been based on simulations of $\sim\!6$ ns, approximately 2500 times less than those found in this study. These studies make the intriguing claim that 50 ps (approximately 300,000 times less than that found in the present study) would be sufficient to estimate free energies for tRNA binding.

The simulation produces an aggregate sampling that is at least 35 times greater than that of earlier drug-binding calculations, which sampled <400 ns,⁴⁴ and 2500 times greater than previous calculations of decoding center/ligand complexes.⁴³ These two studies also used multiple trajectories to achieve aggregate sampling. Furthermore, these estimates, based on the actual simulation time (320 ns per replica), are to be considered conservative. In fact, the REMD methodology has been estimated to actually enhance sampling by 25- to 75-fold.^{29,30}

The type of statistical analysis performed here (Fig. 3) gives only an estimate of the convergence of the landscape and the sampling necessary to obtain such convergence. Our convergence plots (Fig. 3) show that we have reduced sampling artifacts in our free-energy estimates to below 0.2 kcal/mol. Fluctuations in the entropy/enthalpy landscapes are higher than those in the free-energy landscapes, but relative errors are small in this case, given the much larger absolute scales (the relative barriers on these landscapes are generally >5 kcal/mol). Although our simulations are more precise in estimating thermodynamic properties within the framework of a force-field-based model than other simulations that make use of much less sampling, systematic errors due to the force field itself cannot be excluded. These errors become more apparent as sampling increases because they are no longer "blurred out" by statistical errors arising from insufficient sampling. This type of systematic uncertainty cannot be directly measured from the simulations themselves; it can only be estimated by validation through experiment. The global picture of the flipping of A1492 and A1493, the complexity of the binding free-energy landscape, and the even higher complexity of entropy/enthalpy decomposition arising from the simulations is confirmed by the consistency of our results with available experiments.

Methods

Simulated systems

The simulated A-site consists of residues 1404–1411 and 1489–1497 extracted from the *E. coli* ribosome sequence (Fig. 1b). Six different initial structures with different flipping states for residues A1492 and A1493 were used for the simulation of the empty A-site (system S1). These were derived from two *E. coli* ribosomal X-ray structures and four *Thermus thermophilus* ribosomal structures (Table 1). All nucleotides were unmodified, as in the X-ray structures. We note that while 1407 exists as m5C in *E. coli*, this modification has previously been shown to have no effect on gentamicin binding or on associated $K_{\rm d}$. From each of the four *T. thermophilus* structures, an *E. coli* A-site structure was obtained by modeling the mutation of the G1410 = C1490 base pair to A1410 = U1490 using CHIMERA. The initial structure for the gentamicin-bound A-site (system S2) was derived from the 2.8-Å X-ray structure. System S1 consists of the rRNA A-site as defined above, 5324 SPC/E water molecules, 25 K+, 12 Cl-, and 1 Mg²⁺, to which 6 SPC/E

water molecules were bound by a restraining potential forming a hexa-hydrated magnesium ion (MgW₆). When free in solution, magnesium ions are normally (at the timescales accessible by MD) in a hexa-hydrated state. None of the crystal structures used in this study presents bound pentahydrated magnesium ions in the vicinity of the A-site. Our implementation avoids possible artificial binding of the magnesium ion to the RNA in the course of our simulations. Upon computing the correlation coefficient for magnesium proximity to the flipping base and base flipping, we obtain $r \sim 0.03$, demonstrating that little correlation exists between base flipping and magnesium proximity. System S2 differs from S1 in terms of the presence of one gentamicin molecule and the number of K⁺ and Cl⁻ (28 and 19, respectively). This choice results in excess concentrations of ~0.1 M KCl and ~7 mM MgCl₂ for both systems S1 and S2.

Force-field parameters

The X-ray structure of gentamicin from Francois et al. 19 was fully protonated (+5) using the Leap program of the AMBER 8.0 suite. 47 The electrostatic potential was calculated at more than 16,000 points on a molecular surface around the gentamicin molecule from a singlepoint HF/631G* calculation performed on the protonated structure. The set of partial atomic charges for the gentamicin molecule was obtained by fitting the electrostatic potential using the RESP module in the AMBER 8.0 suite.4 All other parameters for gentamicin were generated using the ANTECHAMBER module in AMBER 8.0 and then converted into GROMACS⁴⁸ format. The MgW₆ ion was treated as a separate residue in GROMACS in which the oxygen atoms of six SPC/E water molecules were restrained by bond, angle, and dihedral terms to a standard AMBER magnesium ion. This was done to introduce a certain degree of polarizability to the magnesium ion in order to partially compensate for inaccuracies in describing the interactions between solvated magnesium ions and RNA. 49 The full set of parameters for MgW $_6$ is supplied as Supporting Information in the form of a GROMACS topology file. Van der Waals parameters for Cl⁻ and K⁺ were extracted from Dang^{20,50} and have been extensively tested in combination with the SPC/E water model and AMBER ff99 RNA parameters.²⁸ All other simulation parameters were taken from the ffamber 9951 port of the AMBER 99 force field to GROMACS.

Simulation protocol

Each of the seven structures (Table 1) was aligned and placed at the center of a cubic box that was 55 Å in length. Ions were placed in random positions within the box. A minimum distance of 3.0 Å between ions and solute atoms was imposed. The resulting systems were solvated, and

Table 1. Initial structures for simulations S1 and S2

Structure	PDB accession code	Organism	A1492	φ ₁₄₉₂ [°]	A1493	φ ₁₄₉₃ [°]
1	2AVY	E. coli	In	-39.4	In	-19.3
2	2AW7	E. coli	In	-0.4	Out	-97.4
3	1IBM	T. thermophilus	Out	125.8	Out	130.8
4	1J5E	T. thermophilus	In	4.7	In	5.6
5	1N34	T. thermophilus	In	32.9	Out	122.0
6	1N36	T. thermophilus	In/out	22.0	Out	126.6
7	2ET3	E. coli	Out	96.8	Out	108.4

the $\rm MgW_6$ residue was placed at one corner of the solvated box; the six water molecules closest to this residue were deleted. The seven systems thus obtained were energy-minimized and equilibrated in the course of 1.5 ns to a pressure of 1.0 atm and a temperature of 300 K using an integration time step of 1.5 fs following a well-tested equilibration protocol for MD of RNA systems. ²⁸ In all calculations, long-range electrostatic interactions were calculated using the particle mesh Ewald method. ^{52,53}

In order to mimic the environmental constraints imposed by the rest of the ribosome on the initial structures used for simulation of system S1, the terminal base pairs of the RNA duplex (C1404, C1411, G1489, and G1497) were maintained in their original orientations in all phases of the simulation. Similarly, in the simulation of system S2, the same residues were subject to a 10-kcal/mol Ų harmonic restraint. Imposing such restraints offers the advantage of avoiding complete unfolding of the RNA duplex at high temperatures in the replica phase of the simulation.

For the simulations presented here, 48 replicas with temperatures in the range 276.5<T<447.5 K and an exponential temperature distribution ⁵⁴ were used. The distribution was calculated using the standard GROMACS recipe (as described on page 32 of the GROMACS manual) to obtain a projected exchange probability of 0.135 in the desired temperature interval.

Simulations were performed with the GROMACS package, using 240/480 processors on the Coyote machine in Los Alamos. The 48 replicas for simulation S1 were derived from eight copies of the six systems equilibrated at 300 K; these were run without exchanges for an additional 1.5 ns at constant volume each at their respective replica temperature. A similar procedure was followed for the gentamicin simulation (S2). At this point, both simulations were set into full replica exchange mode, with exchanges attempted every 125 steps. All replica simulations were conducted at constant volume. An additional 1.5 ns of simulation time was discarded before actual data collection. System S1 was allowed to run in production mode for 21 ns per replica for a total sampling of more than 1 μs. Production time on system S2 was 320 ns per replica for a total of more than 15 μs.

Potential of mean force

A pseudo-dihedral angle ϕ (Fig. 1d), originally defined by Huang and MacKerell, was used to distinguish flipped-in/flipped-out states for A1492 and A1493. For any given base, the angle ϕ is defined as the dihedral angle formed by the centers-of-mass of: (i) the neighboring base pair; (ii) the neighboring sugar; (iii) the sugar of the base itself; and (iv) the base. A second pair of coordinates ($R_{\rm CM}$ and $R_{\rm X}$) was used to describe the binding/unbinding of gentamicin to the A-site. The first, $R_{\rm CM}$, is defined as the distance between the position of the gentamicin center-of-mass, as derived from the crystallographic structure, and its position along the simulation trajectory. The second, $R_{\rm X}$, is defined as:

$$R_X = \frac{1}{9} \sqrt{\sum_{i=1}^{9} (r_i^{\text{sim}} - r_i^{\text{ref}})^2}$$
 (2)

where r_i^{ref} {i=1...9} refers to the set of nine closest RNA/gentamicin crystal contact distances described in Fig. 1c. Similarly, r_i^{sim} refers to the same set of distances as they occur in the course of the simulation.

The PMF can be approximated by MD simulations from the probability P(a,b,T) of finding the system in a given

state within the subspace of states spanned by the reaction coordinates a and b at a given temperature T:⁴²

$$\Delta G(a, b, T) = -kT \ln[P(a, b, T)] \tag{3}$$

REMD simulations also provide the temperature dependence of $\Delta G(a,b,T)$, which was used here to separate enthalpic from entropic contributions to the free energy at T_0 =300 K^{40,56} for dissociation of gentamicin from the binding site. This is achieved by fitting the thermodynamic formula:

$$\Delta G = \Delta H - T\Delta S$$

$$\Delta H = \Delta H_0 + \int_{T_0}^{T} \Delta C_v d\Theta$$

$$\Delta S = \Delta S_0 + \int_{T_0}^{T} \frac{\Delta C_v}{\Theta} d\Theta$$

$$\Delta C_v = \Delta C_v^0 + (T - T_0) \left[\frac{d\Delta C_v}{dT} \right]_0$$
(4)

where C_v is the heat capacity at constant volume, H is enthalpy, and S is entropy.

Calibration by time-resolved fluorescence experiments

The results of experiments by Kaul *et al.* performed on a fluorescent analog of the A-site were used to calibrate the landscape of Fig. 2a using the working hypothesis described schematically in Fig. 7.²⁶

The normalized amplitudes for the three distinct fluorescent states, a_{LU} =0.076, a_{MU} =0.098, and a_{SU} =0.826, were used to assign sections of the free-energy landscape to the three states. For the case of simulation S1 (Fig. 2a), these three states correspond to the three different stacking configurations of points (i)-(iii) described in the Fig. 6 caption. The landscape was initially divided into three areas characterized by $\phi_{1492,min}$ =-60° and $\phi_{1492,max}$ =60°, which bound the minimum at $\phi_{1492} = 0^{\circ}$. These values were iteratively adjusted in 1° steps in order to obtain exactly a fraction a_{SU} of all configurations of the simulation with $\phi_{1492,min}$ < ϕ_{1492} < $\phi_{1492,max}$ (area labeled L_U in Fig. 2a). The values obtained for $\phi_{1492,min}$ and $\phi_{1492,max}$ were -55° and 41°, respectively. Similarly, two values of ϕ_{1493} were used and iteratively refined to distinguish sections M_U and S_U in Fig. 2a. The final values of $\phi_{1493,min}$ and $\phi_{1493,max}$ were -8° and 31°, respectively.

Acknowledgements

The authors are grateful to Angel Garcia, Andy White, Manuel Vigil, Marcus Daniels, Dirk Herten, and Dmitri Babikov for their support and input. We are grateful to the referees for improving our manuscript. This work was performed under the auspices of the US Department of Energy under contract W-7405-ENG-36. K.Y.S. and A.C.V. were supported by National Institutes of Health grant R01-GM072686. The Ribosome Project was generously supported by the Los Alamos National Laboratory Institutional Computing Program.

Supplementary Data

Supplementary data associated with this article can be found, in the online version, at doi:10.1016/j.jmb.2008.12.035

References

- 1. Mankin, A. (2006). Antibiotic blocks mRNA path on the ribosome. *Nat. Struct. Mol. Biol.* **13**, 858–860.
- Carter, A. P., Clemons, W. M., Brodersen, D. E., Morgan-Warren, R. J., Wimberly, B. T. & Ramakrishnan, V. (2000). Functional insights from the structure of the 30S ribosomal subunit and its interactions with antibiotics. *Nature*, 407, 340–348.
- 3. Wimberly, B. T., Brodersen, D. E., Clemons, W. M., Jr, Morgan-Warren, R. J., Carter, A. P., Vonrhein, C. *et al.* (2000). Structure of the 30S ribosomal subunit. *Nature*, **407**, 327–339.
- Schuwirth, B. S., Borovinskaya, M. A., Hau, C. W., Zhang, W., Vila-Sanjurjo, A., Holton, J. M. & Cate, J. H. (2005). Structures of the bacterial ribosome at 3.5 A resolution. *Science*, 310, 827–834.
- Korostelev, A., Trakhanov, S., Laurberg, M. & Noller, H. F. (2006). Crystal structure of a 70S ribosome-tRNA complex reveals functional interactions and rearrangements. *Cell*, 126, 1065–1077.
- 6. Plant, E. P., Nguyen, P., Russ, J. R., Pittman, Y. R., Nguyen, T., Quesinberry, J. T. *et al.* (2007). Differentiating between near- and non-cognate codons in Saccharomyces cerevisiae. *PLoS ONE*, **2**, e517.
- 7. Yoshizawa, S., Fourmy, D. & Puglisi, J. D. (1999). Recognition of the codon-anticodon helix by ribosomal RNA. *Science*, **285**, 1722–1725.
- 8. Ogle, J. M., Brodersen, D. E., Clemons, W. M., Jr, Tarry, M. J., Carter, A. P. & Ramakrishnan, V. (2001). Recognition of cognate transfer RNA by the 30S ribosomal subunit. *Science*, **292**, 897–902.
- 9. Ogle, J. M., Murphy, F. V., Tarry, M. J. & Ramakrishnan, V. (2002). Selection of tRNA by the ribosome requires a transition from an open to a closed form. *Cell*, **111**, 721–732.
- Ogle, J. M. & Ramakrishnan, V. (2005). Structural insights into translational fidelity. *Annu. Rev. Biochem.* 74, 129–177.
- 11. Sanbonmatsu, K. Y. & Joseph, S. (2003). Understanding discrimination by the ribosome: stability testing and groove measurement of codon-anticodon pairs. *J. Mol. Biol.* **328**, 33–47.
- VanLoock, M. S., Easterwood, T. R. & Harvey, S. C. (1999). Major groove binding of the tRNA/mRNA complex to the 16 S ribosomal RNA decoding site. J. Mol. Biol. 285, 2069–2078.
- 13. Lim, V. I. & Curran, J. F. (2001). Analysis of codon: anticodon interactions within the ribosome provides new insights into codon reading and the genetic code structure. *Rna*, 7, 942–957.
- Yoshizawa, S., Fourmy, D. & Puglisi, J. D. (1998). Structural origins of gentamicin antibiotic action. EMBO J. 17, 6437–6448.
- Fourmy, D., Yoshizawa, S. & Puglisi, J. D. (1998).
 Paromomycin binding induces a local conformational change in the A-site of 16S rRNA. J. Mol. Biol. 277, 333–345
- Fourmy, D., Recht, M. I., Blanchard, S. C. & Puglisi, J. D. (1996). Structure of the A site of Escherichia coli

- 16S ribosomal RNA complexed with an aminoglycoside antibiotic. *Science*, **274**, 1367–1371.
- 17. Selmer, M., Dunham, C. M., Murphy, F. V. t., Weixlbaumer, A., Petry, S., Kelley, A. C. *et al.* (2006). Structure of the 70S ribosome complexed with mRNA and tRNA. *Science*, **313**, 1935–1942.
- Vicens, Q. & Westhof, E. (2002). Crystal structure of a complex between the aminoglycoside tobramycin and an oligonucleotide containing the ribosomal decoding A site. Chem. Biol. 9, 747–755.
- A site. *Chem. Biol.* **9**, 747–755.

 19. Francois, B., Russell, R. J., Murray, J. B., Aboul-ela, F., Masquida, B., Vicens, Q. & Westhof, E. (2005). Crystal structures of complexes between aminoglycosides and decoding A site oligonucleotides: role of the number of rings and positive charges in the specific binding leading to miscoding. *Nucleic Acids Res.* **33**, 5677–5690.
- 20. Dang, L. X. (1995). Mechanism and thermodynamics of ion selectivity in aqueous solutions of 18-crown-6 ether: a molecular dynamics study. *J. Am. Chem. Soc.* **117**, 6954–6960.
- Daviter, T., Gromadski, K. B. & Rodnina, M. V. (2006).
 The ribosome's response to codon-anticodon mismatches. *Biochimie*, 88, 1001–1011.
- Rodnina, M. V. & Wintermeyer, W. (2001). Fidelity of aminoacyl-tRNA selection on the ribosome: kinetic and structural mechanisms. *Annu. Rev. Biochem.* 70, 415–435.
- Sanbonmatsu, K. Y. (2006). Energy landscape of the ribosomal decoding center. *Biochimie*, 88, 1053–1059.
- 24. Lynch, S. R., Gonzalez, R. L. & Puglisi, J. D. (2003). Comparison of X-ray crystal structure of the 30S subunit-antibiotic complex with NMR structure of decoding site oligonucleotide-paromomycin complex. *Structure*, **11**, 43–53.
- Koshland, D. E. (1958). Application of a Theory of Enzyme Specificity to Protein Synthesis. *Proc. Natl Acad. Sci. USA*, 44, 98–104.
- Kaul, M., Barbieri, C. M. & Pilch, D. S. (2006). Aminoglycoside-induced reduction in nucleotide mobility at the ribosomal RNA A-site as a potentially key determinant of antibacterial activity. *J. Am. Chem.* Soc. 128, 1261–1271.
- Ravindranathan, K. P., Gallicchio, E., Friesner, R. A., McDermott, A. E. & Levy, R. M. (2006). Conformational equilibrium of cytochrome P450 BM-3 complexed with N-palmitoylglycine: a replica exchange molecular dynamics study. *J. Am. Chem. Soc.* 128, 5786–5791.
- Vaiana, A. C., Westhof, E. & Auffinger, P. (2006). A molecular dynamics simulation study of an aminoglycoside/A-site RNA complex: conformational and hydration patterns. *Biochimie*, 88, 1061–1073.
- Sanbonmatsu, K. Y. & Garcia, A. E. (2002). Structure of Met-enkephalin in explicit aqueous solution using replica exchange molecular dynamics. *Proteins*, 46, 225–234.
- Zhang, W., Wu, C. & Duan, Y. (2005). Convergence of replica exchange molecular dynamics. *J. Chem. Phys.* 123, 154105.
- Garcia, A. E. & Sanbonmatsu, K. Y. (2002). Alphahelical stabilization by side chain shielding of backbone hydrogen bonds. *Proc. Natl Acad. Sci. USA*, 99, 2782–2787.
- Garcia, A. E. & Sanbonmatsu, K. Y. (2001). Exploring the energy landscape of a beta hairpin in explicit solvent. *Proteins*, 42, 345–354.
- Gnanakaran, S., Nymeyer, H., Portman, J., Sanbonmatsu, K. Y. & Garcia, A. E. (2003). Peptide folding simulations. *Curr. Opin. Struct. Biol.* 13, 168–174.

- 34. Garcia, A. E. & Paschek, D. (2008). Simulation of the pressure and temperature folding/unfolding equilibrium of a small RNA hairpin. *J. Am. Chem. Soc.* **130**, 815–817.
- 35. Kaul, M., Barbieri, C. M. & Pilch, D. S. (2005). Defining the basis for the specificity of aminoglycoside-rRNA recognition: a comparative study of drug binding to the A sites of Escherichia coli and human rRNA. *J. Mol. Biol.* **346**, 119–134.
- Kopelevich, D. I., Panagiotopoulos, A. Z. & Kevrekidis, I. G. (2005). Coarse-grained kinetic computations for rare events: application to micelle formation. *J. Chem. Phys.* 122, 44908.
- 37. Yang, S., Onuchic, J. N. & Levine, H. (2006). Effective stochastic dynamics on a protein folding energy landscape. *J. Chem. Phys.* **125**, 054910.
- McCammon, J. A., Wolynes, P. G. & Karplus, M. (1979). Picosecond dynamics of tyrosine side chains in proteins. *Biochemistry*, 18, 927–942.
 Qian, H. & Hopfield, J. J. (1996). Entropy-enthalpy
- Qian, H. & Hopfield, J. J. (1996). Entropy-enthalpy compensation: Perturbation and relaxation in thermodynamic systems. J. Chem. Phys. 105, 9292–9298.
- Nymeyer, H., Woolf, T. B. & Garcia, A. E. (2005). Folding is not required for bilayer insertion: replica exchange simulations of an alpha-helical peptide with an explicit lipid bilayer. *Proteins*, 59, 783–790.
- 41. Tovchigrechko, A. & Vakser, I. A. (2001). How common is the funnel-like energy landscape in protein-protein interactions? *Protein Sci.* 10, 1572–1583.
- Vaiana, A. C., Neuweiler, H., Schulz, A., Wolfrum, J., Sauer, M. & Smith, J. C. (2003). Fluorescence quenching of dyes by tryptophan: interactions at atomic detail from combination of experiment and computer simulation. J. Am. Chem. Soc. 125, 14564–14572.
- Almlof, M., Ander, M. & Aqvist, J. (2007). Energetics of codon-anticodon recognition on the small ribosomal subunit. *Biochemistry*, 46, 200–209.
- 44. Fujitani, H., Tanida, Y., Ito, M., Jayachandran, G., Snow, C. D., Shirts, M. R. *et al.* (2005). Direct calculation of the binding free energies of FKBP ligands. *J. Chem. Phys*, **123**, 084108.

- Wong, C. H., Hendrix, M., Priestley, E. S. & Greenberg, W. A. (1998). Specificity of aminoglycoside antibiotics for the A-site of the decoding region of ribosomal RNA. *Chem. Biol.* 5, 397–406.
- Pettersen, E. F., Goddard, T. D., Huang, C. C., Couch, G. S., Greenblatt, D. M., Meng, E. C. & Ferrin, T. E. (2004). UCSF Chimera–a visualization system for exploratory research and analysis. *J. Comput. Chem.* 25, 1605–1612.
- Case, D., Darden, T. A., Cheatham, T. E., Simmerling, C. L., Wang, J., Duke, R. E. et al. (2004). AMBER 8. University of California, San Francisco.
- Van Der Spoel, D., Lindahl, E., Hess, B., Groenhof, G., Mark, A. E. & Berendsen, H. J. (2005). GROMACS: fast, flexible, and free. J. Comput. Chem. 26, 1701–1718.
- Petrov, A. S., Pack, G. R. & Lamm, G. (2004).
 Calculations of magnesium Nucleic acid site binding in solution. *J. Phys. Chem. B*, 108, 6072–6081.
- Dang, L. X. (1994). Free Energy of Assocciation of Cs+ to 18-Crown-6 in Water. A Molecular Dynamics Study Including Counter Ions. Chem. Phys. Lett. 227, 211–214.
- 51. Sorin, E. J. & Pande, V. S. (2005). Exploring the helix-coil transition via all-atom equilibrium ensemble simulations. *Biophys. J.* **88**, 2472–2493.
- 52. Darden, T., York, D. & Pedersen, L. (1993). Particle mesh Ewald: an N.log(N) method for Ewald sums in large systems. *J. Chem. Phys.* **98**, 10089–10092.
- Essmann, U., Perera, L., Berkowitz, M. L., Darden, T., Lee, H. & Pedersen, L. G. (1995). A smooth particle mesh Ewald method. J. Chem. Phys. 103, 8577–8593.
- 54. Nymeyer, H., Gnanakaran, S. & Garcia, A. E. (2004). Atomic simulations of protein folding, using the replica exchange algorithm. *Methods Enzymol.* **383**, 119–149.
- 55. Huang, N. & MacKerell, A. D., Jr (2004). Atomistic view of base flipping in DNA. *Philos. Transact. A Math Phys. Eng. Sci.* **362**, 1439–1460.
- Nymeyer, H. & Garcia, A. E. (2003). Simulation of the folding equilibrium of alpha-helical peptides: a comparison of the generalized Born approximation with explicit solvent. *Proc. Natl Acad. Sci. USA*, 100, 13934–13939.